OPEN ACCESS

University of BRISTOL

Peer reviewed version

License (if available):
Unspecified

Link to published version (if available):
10.1016/j.matchar.2017.07.038

Link to publication record in Explore Bristol Research

PDF-document

University of Bristol - Explore Bristol Research

General rights

Specimen preparation methods for elemental characterisation of grain boundaries and isolated dislocations in multicrystalline silicon using atom probe tomography

C. Lotharukpong[1], D. Tweddle[1], T.L. Martin[2], M. Wu[1], C.R.M. Grovenor[1], M.P. Moody[1], P.R. Wilshaw[1*]

[1]*University of Oxford, Department of Materials, Parks Road, Oxford, OX1 3PH, UK.*
[2]*Interface Analysis Centre, School of Physics, University of Bristol, Tyndall Avenue, Bristol BS8 1TL, UK*

[*]email: peter.wilshaw@materials.ox.ac.uk tel: +447966786171 fax: +441865273789

Abstract

Multicrystalline silicon (mc-Si) is a cost effective feedstock for solar photovoltaic devices but is limited by the presence of defects and impurities. Imaging impurities segregated to nanometre-scale dislocations and grain boundaries is a challenge that few materials characterisation techniques can achieve. Atom Probe Tomography (APT) is a 3-dimensional time-of-flight microscopy technique that can image the distribution of elements at the atomic scale, however one of the most challenging factors when using APT is the complexity of specimen preparation for specific regions of interest. Atom probe specimen preparation methods have been developed in a dual FIB/SEM system that enable a specific extended defect such as an isolated dislocation or a section of a grain boundary to be selected for APT analysis. The methods were used to fabricate APT specimens from an isolated dislocation and a grain boundary in mc-Si samples. Complementary TEM images confirm the presence of the defects in both specimens, whilst APT analyses also reveal segregation of impurities to the defects.

Keywords: atom probe tomography; focused ion beam; grain boundaries; isolated dislocations; multicrystalline silicon

1. Introduction

The photovoltaic industry has in recent years been dominated by the use of multicrystalline silicon (mc-Si) solar cells, which offer substantial cost reduction compared to monocrystalline silicon bulk material. However, the presence of high densities of defects such as dislocations, grain boundaries (GB) and stacking faults in multicrystalline silicon leads to more possible recombination centres for electron-hole pairs created during operation, reducing the efficiency of the solar cell, from a record efficiency of 25.6% for single crystal silicon to a maximum of 21.25% for mc-Si[1].

The decrease in efficiency of mc-Si solar cells has been linked to the density of dislocations and impurities, and the segregation of impurity atoms such as Fe, Cr, Ni and Cu to them[2]. New mc-Si growth

1

methods have reduced the grain boundary density[3] and the dendrite casting method that induces <110> and <112> dendrite growth along the crucible bottom has also been demonstrated to grow large grains with a high number of electrically inactive Σ3 twin boundaries[4] that also reduce the dislocation density.[5] Nevertheless, recombination at dislocations and GBs still limits the efficiency of mc-Si solar cells. For many years, gettering has been used to remove transition metal impurities, in particular using phosphorus diffusion during high-temperature processing to draw the impurities to the phosphorus rich region forming metal rich precipitates at the surface. Whilst it has been demonstrated using bulk chemical characterisation techniques that increased metal content reduces cell efficiency[6,7], characterising the distribution of these impurities to atomic-scale defects pre- and post-gettering remains a challenge. Whilst synchrotron-based nanoprobe X-ray fluorescence mapping has been able to image larger defects[8], it can only obtain a resolution of 80 nm[9], insufficient to image the distribution of impurity atoms on individual defects in mc-Si.

In recent years atom probe tomography (APT) has become a valuable nanoscale characterisation tool for the development of new silicon-based semiconductor materials and devices, particularly as the scale of such devices shrink. For example, there are few techniques that can image the 3D chemical distribution across entire individual transistors[10]. The implementation of laser pulsing capabilities in atom probe instruments has been critical in opening up APT to a much wider range of semiconductor materials applications[11]. However, a concurrent advance in the development of site-specific Focused Ion Beam (FIB) based techniques[12], to prepare the very sharp needle-shaped specimens required by APT, was equally important.

The development of FIB/SEM dual-beam systems enables the combination of milling with the ion beam, and imaging with the electron beam, in order to fabricate atom probe specimens with a much greater degree of control over the final tip shape and location. The standard preparation method is the FIB lift-out technique, where a small piece of the sample is removed from the bulk sample, transferred to a support structure and sharpened into a needle[12,1314].

Numerous adaptations of the FIB lift-out process have been reported in the literature that allow APT specimens to be made from a specific region of interest (RoI). The characterisation of dopant and impurity segregation in silicon using APT has shown boron clusters at the intersection of grains[15,16], nickel segregation to dislocation loops in ion-implanted silicon wafers[17] and the segregation of P, As, C and O to grain boundaries in annealed multicrystalline silicon[18]. Recently an atom probe specimen preparation method developed by Stoffers and co-workers[19] was able to demonstrate the ability to extract grain boundaries from mc-Si samples in a reproducible manner. This was achieved by adapting a TEM-based preparation method developed by Felfer et al[20], where the specimen containing a grain boundary is lifted and mounted onto a TEM grid and imaged using a TEM to identify the position of the defect. The specimen is then returned to the FIB for final polishing to precisely position the grain boundary at the tip apex for APT analysis. However, in addition to the time-intensity of the process, since the grain boundary is located perpendicular to the field evaporation direction in the APT analysis, specimens fabricated using this approach only contain a small section of the grain boundary. This limits the probability of precipitates and individual dislocations in the analysis, which may be distributed along grain boundaries within the bulk material.

Significantly, the Stoffers method is also only suitable for grain boundaries, rather than isolated dislocations. These defects are thought to play an important role in the segregation of undesirable impurities[21] however, dislocations are much more widely distributed and are generally thought to be a more important limiting factor in cell efficiency[5]. Hence it is critical to have a specimen preparation technique with the ability to identify, select and incorporate specific isolated dislocations for APT analysis. Using the traditional top-down liftout method to obtain an isolated dislocation in the analysis

volume is extremely challenging. This is because the dislocation does not necessarily extend vertically down from the surface, and also the annular milling to create the needle specimen can result in etching away the desired feature.

This paper presents in detail two novel atom probe specimen preparation methods, based on a rotated form of the lift-out technique, for extracting isolated dislocations and grain boundaries from mc-Si subjected to different processing conditions. Complementary TEM was carried out to confirm the feature of interest was present in the fabricated specimen prior to APT analysis. Finally, the resulting APT reconstructions demonstrate the effectiveness of the techniques developed, to facilitate the characterisation of the mc-Si microstructure. The selective nature of this approach can also be combined with other characterisation such as electron beam induced current (EBIC) to link the structure and chemical segregation of a defect to its electrical activity. Although this paper demonstrates the method for the analysis of mc-Si, the specimen preparation methods described here could also be used to isolate and analyse individual selected dislocations and grain boundaries in other materials which have dislocations oriented roughly perpendicular to the sample surface.

2. Materials and Methods

This study examined p-type mc-Si wafers produced by REC Solar. Samples were taken from the top region of a commercial ingot produced by directional solidification, and subsequently diced into 5mm square pieces.

For the purpose of proving that APT can successfully image dislocations at grain boundaries, a wafer of mc-Si was intentionally contaminated with gold. The sample was mechanically polished using 8, 1 and 0.25 micron polishing pads to remove saw damage regions, followed by chemo-mechanically polishing using a Chem-H polishing pad. Surface contaminants and oxide were removed using RCA and HF cleans respectively. A ~50 nm layer of gold was deposited on the surface, followed by annealing in argon gas at 1000 °C for one hour and oil quenching, which is predicted to produce a gold concentration near the wafer surface greater than ~50% of its solid solubility value of ~10^{16} atoms/cm^3.[22]

In order to analyse the segregation of impurities to dislocations after gettering, Phosphorus Diffusion Gettering (PDG) was performed on another mc-Si specimen, which was annealed at 875 °C for 22 min in the presence of 650 sccm $POCl_3$, 500 sccm O_2 and 13.5 SLPM N_2. Subsequently the $POCl_3$ and O_2 flows were turned off and the specimen was cooled to 800°C in an N_2 atmosphere at a rate of 10 °C/min, before removing the specimen from the furnace and cooling to room temperature. Prior to FIB analysis, the phosphorus silicate glass and phosphorus-rich region at the surface were removed by exposure to hot hydrochloric acid for ten minutes followed by two hours of chemo-mechanical polishing.

FIB liftouts were carried out in a Zeiss NVision 40 FIB-SEM system. Defects were lifted-out of the bulk sample using an in-situ Kleindiek nano-manipulator. A gas-injector was used in conjunction with SEM and FIB to deposit carbon and/or tungsten to protect the sample from Ga$^+$ damage and weld the liftout to the manipulator. An Omiprobe© lift-out grid containing five copper posts was used as a support structure for mounting the sample and mounted in a dedicated holder, as previously demonstrated by Felfer *et al*[14]. FIB milling was undertaken using an accelerating voltage of 30 kV, with the exception of a final polishing step at 5 kV. The support structure during wedge attachment and preparation was positioned such that the copper posts are normal to the SEM column axis. During Specimen sharpening, the grid was held at 54° tilt such that the copper posts are parallel to the FIB column axis.

TEM images of the specimens were taken in bright field mode in a double-tilt holder Philips JEOL 2000FX microscope at an accelerating voltage of 200 kV. After characterisation in the TEM, APT analysis was carried out using a Cameca LEAP 3000X HR equipped with an energy-compensated reflectron, and an ultra-high frequency laser which operates at the wavelength of 532 nm. Experiments were performed in an ultra-high vacuum environment of better than $3x10^{-11}$ Torr, and cooled to a specimen temperature of 50 K. APT analyses were carried out using a 0.5 nJ laser beam energy, 0.3% evaporation rate and 160 kHz pulse frequency.

3. The specimen preparation procedure
3.1 Defect marking techniques

Prior to FIB processing, preferential etching of the sample is required so that extended defects are observable via SEM. The bulk silicon sample is mechanically and chemo-mechanically polished to create a smooth surface, and surface contaminants removed using the standard RCA cleaning procedure[23]. In the final step, the sample is submerged in a Secco etch ((49%)HF:(0.05M)$K_2Cr_2O_7$ at a ratio of 1:2) at 20 °C for 30 sec, resulting in pits at the surface that highlight the position of dislocations and GBs. The size and geometry of the pits depends on the etch conditions used. These conditions were optimised to produce etched features with an approximate average width of 100nm and depth of 170nm. This leaves a GB or dislocation far enough below the material surface to reliably retain in the final APT specimen needle.

Figure 1 shows a schematic of the overall liftout process. First, a dislocation pit is identified and marked with a tungsten dot and a layer of carbon to protect it from subsequent damage from the gallium beam. Then, the sample is cut into a wedge using the FIB and lifted out using a nanomanipulator, before mounting onto a TEM half-grid. The key difference with a traditional liftout is that as in Figure 1 (c), the liftout is mounted in a different orientation. Typically in a standard APT liftout, the original surface of the material remains facing upwards in the final needle, whereas in this method the wedge is mounted side-on to the TEM grid such that the original surface is perpendicular to the end of the needle. This is key as it allows the tungsten dot marking the dislocation to be observed during the final polishing of the needle (as in Figure 1(d) and (e)), enabling the user to place the dislocation at the very tip of the final needle used in APT analysis.
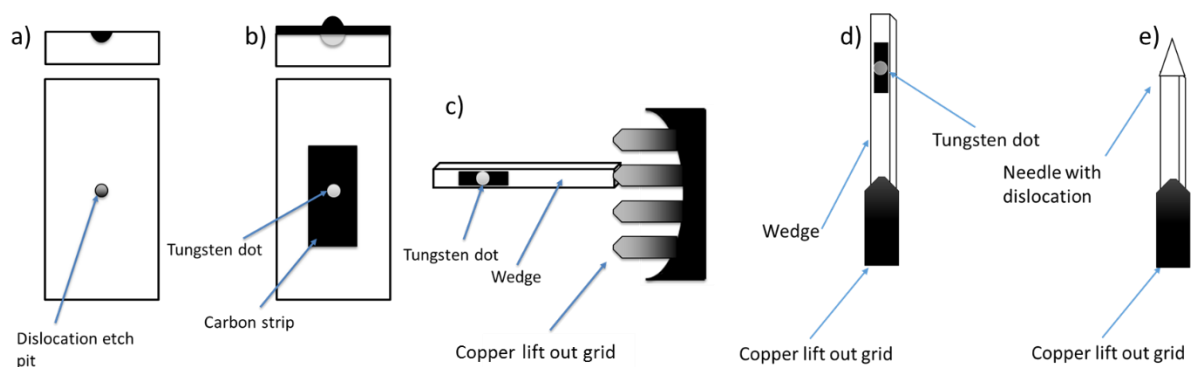

Figure 1. Schematic of the atom probe lift out process. a) dislocation etch pit formed by SECCO etching, b) etch pit is filled by electron deposition tungsten and then a ion deposited carbon strip to protect from gallium damage, c) wedge containing dislocation is lifted out using FIB methods and welded horizontally onto a copper lift out grid, d) copper lift out grid is rotated to align with the FIB column, e) sample is annular milled into a sharp needle, with the dislocation present within 150nm of the tip.

The procedure for marking an isolated dislocation is shown in more detail schematically in Figure 2 (a), and for a grain boundary in Figure 2(b). Although etched defects can easily be observed in both

SEM and FIB, they are vulnerable to the ion beam in subsequent fabrication steps. Therefore, after transferring the sample into the FIB, the next step is to deposit tungsten/carbon onto the features, both for protection and to mark the location of the defects. In the case of an isolated dislocation, a tungsten dot is deposited directly over an isolated dislocation via electron-beam, at 5 kV accelerating voltage and 30 µm objective aperture size. The result is a tungsten fiducial mark around 100 nm in diameter and 200 nm in height. Subsequently a 15x4x0.15 µm carbon protective layer is FIB beam deposited directly over the tungsten dot. Figure 2 (b) shows an isolated dislocation pit after the marking process. The tungsten dot lies in the centre of a carbon dome which provides additional resistance to FIB irradiation.
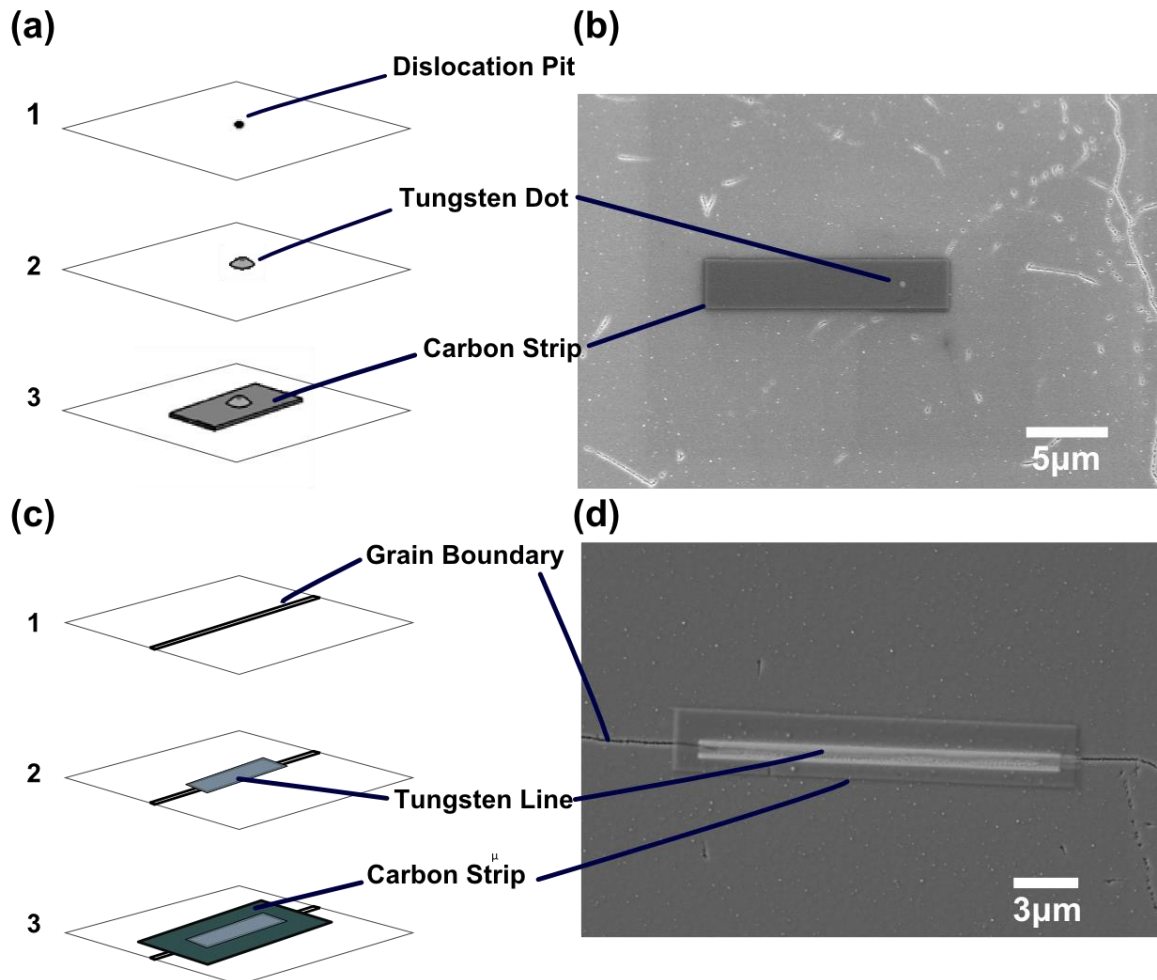

Figure 2. (a) A schematic showing the defect marking procedure for the dislocation pit; and (b) is an SEM image showing a dislocation pit after the marking process. (c) defect marking procedure for the etched grain boundary; and (d) is an SEM image of a grain boundary after the marking process.

A similar approach is employed for marking a specific section of a grain boundary, as shown in Figure 2 (c). First, a line of tungsten is deposited to fill the etched cavity of the grain boundary. A low ion beam current of 1 pA is used in this step in order to reduce damage to the silicon below the etch pit. The length of the tungsten line is dependent on the length of the section of the grain boundary to be analysed. As before, a thin layer of carbon is applied over the tungsten marker using the FIB. An example of a grain boundary marked using this technique is shown in Figure 2 (d).

3.2 Wedge Lift-out and attachment

Once the defect has been marked and protected, a cantilever is fabricated to prepare the region containing the defect for the lift-out. Due to the difference in mounting to the TEM post, the geometry of this cantilever varies from the traditional APT liftout[12], as shown in Figure 3. First, a 2x32x5 μm undercut trench is created along the length of the carbon strip by milling a rectangular pattern at 45° relative to the sample surface (a stage tilt of 9°). The sample is rotated by 180° and the same step is repeated at the other side of the strip. A 10x2x5 μm vertical cut is then created at the end of the carbon strip to create a wedge of cantilever geometry for liftout. All the milling processes are performed with an ion beam current of 3 nA. The undercut trenches are repeated at a lower beam current of 300 pA to ensure that the bottom part of the wedge is completely detached from the bulk sample. Once a cantilever is fabricated, the loose end to wedge is attached to the nano-manipulator. A cut is then made and the wedge is lifted-out of the bulk sample.
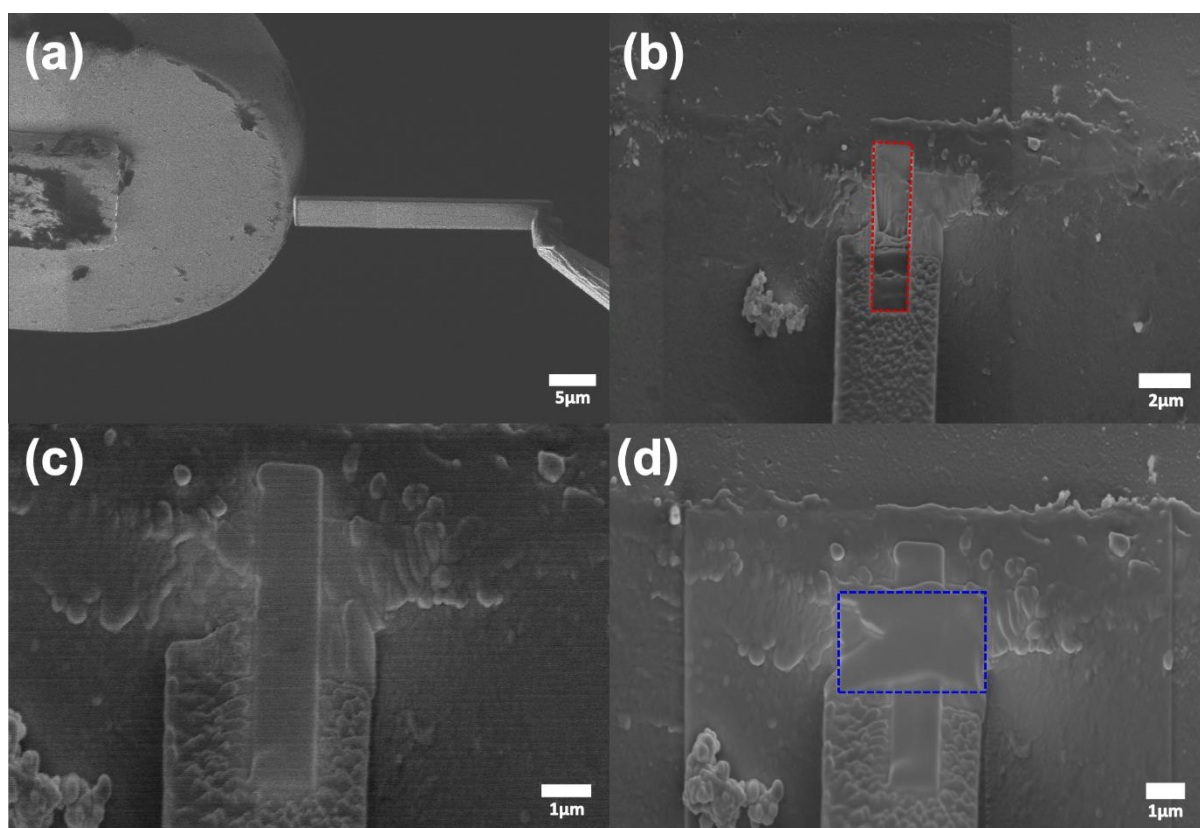

Figure 3 (a) The wedge is mounted to the copper post in an end-to-end manner. (b)–(d). Illustration of the procedure used to reinforce the attachment between the wedge and the copper post: (a) a rectangular hole is partially milled at the interface between the wedge and the post, marked by the dashed red rectangle; (b) the hole is filled with tungsten by FIB deposition; and (c) a tungsten bar is FIB-deposited parallel to the interface, marked by the dashed blue rectangle.

Figure 3 (b-d) shows the methodology for welding the liftout to the TEM needle to ensure a robust connection able to survive the APT process. As the liftout bar is being mounted perpendicular to the TEM post, a traditional weld on either side of the triangular cross-section is not possible. Instead, a cross-shaped weld is used, where first a 700 pA cut is made into the centre of both the liftout and TEM needle and filled with tungsten, and then a second rectangular weld is made perpendicular to this first weld, at the interface between the two materials.

3.3 Wedge preparation

The next stage is to remove material from the end of the wedge so that the defect of interest is within a few hundred nanometres of the end – i.e. within a volume suitable for APT analysis. The extent of this reduction depends on the defect type being analysed. For the isolated dislocation, the height of the wedge is gradually removed at a beam current of 80 pA until the edge is about 300–400 nm from the centre of the marker. This allows sufficient volume of the wedge that if the dislocation pit propagates towards the end of the wedge, it will remain within the final tip volume. Figure 4 (a) and (b) show the wedge before and after the removal process, respectively. For the grain boundary, the top section of the wedge was removed until it reached the tungsten line-marker, as illustrated in Figure 4 (c) and (d).
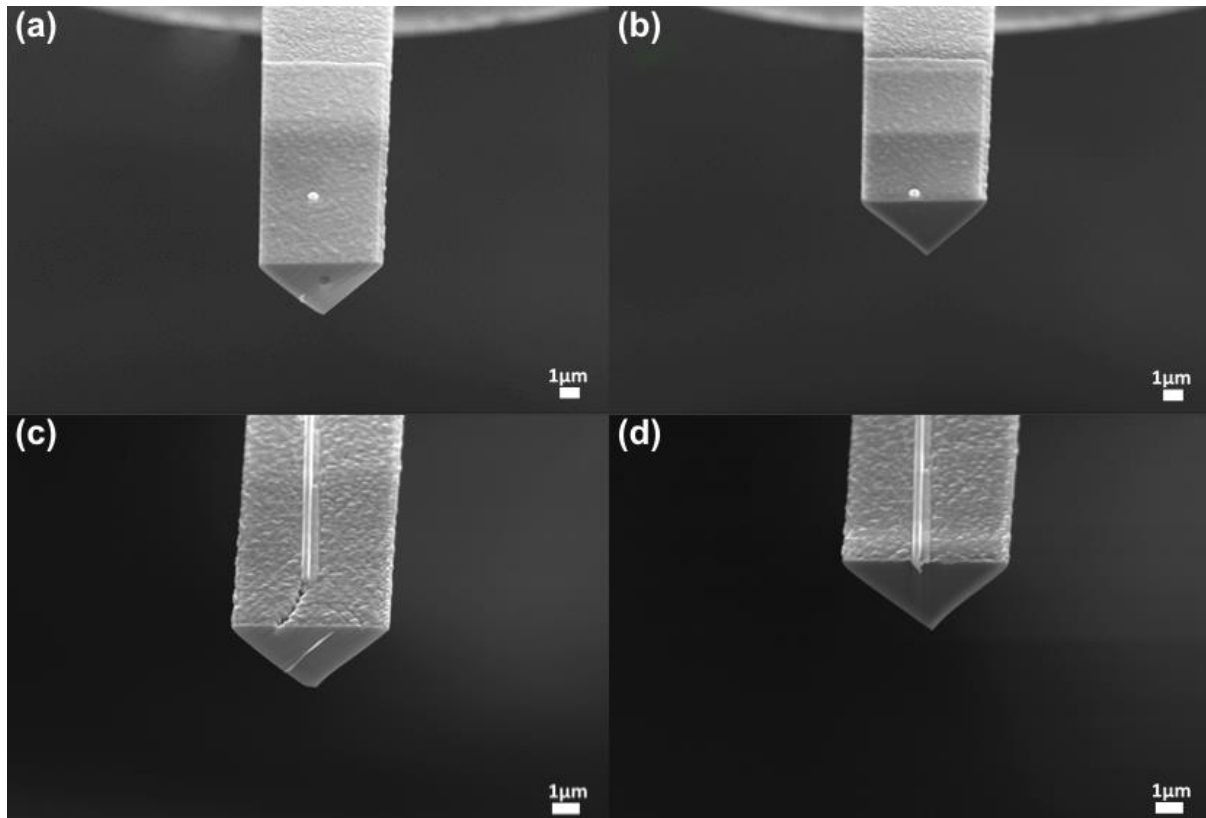

Figure 4. SEM images showing a wedge containing a marked dislocation pit (a) before and (b) after excess height was removed. (c) and (d) show the same process for a grain boundary, with a section marked by a tungsten line.

3.4 Specimen sharpening

The specimen sharpening procedure is shown schematically in Figure for the isolated dislocation and Figure 6 (a) for a grain boundary. For the isolated dislocation, first at 54⁰ tilt a rectangular pattern is applied to the front surface of the specimen, moving progressively in towards the specimen from the original surface until only a small portion of the dislocation pit can be observed, but the bottom of the tungsten fiducial mark is still visible. The wedge is then sharpened into an APT needle-shaped specimen by applying a series of annular milling patterns. The milling beam current is systematically decreased from 3 nA to 40 pA as the inner diameter of the annular milling pattern becomes smaller. In addition, the distances between the centres of the dislocation to the edges are measured after each annular milling step to ensure that the dislocation line intersects with the specimen once the needle is formed. A 5 kV polish is then used to further sharpen the needle and minimise gallium damage at the surface of the specimen.
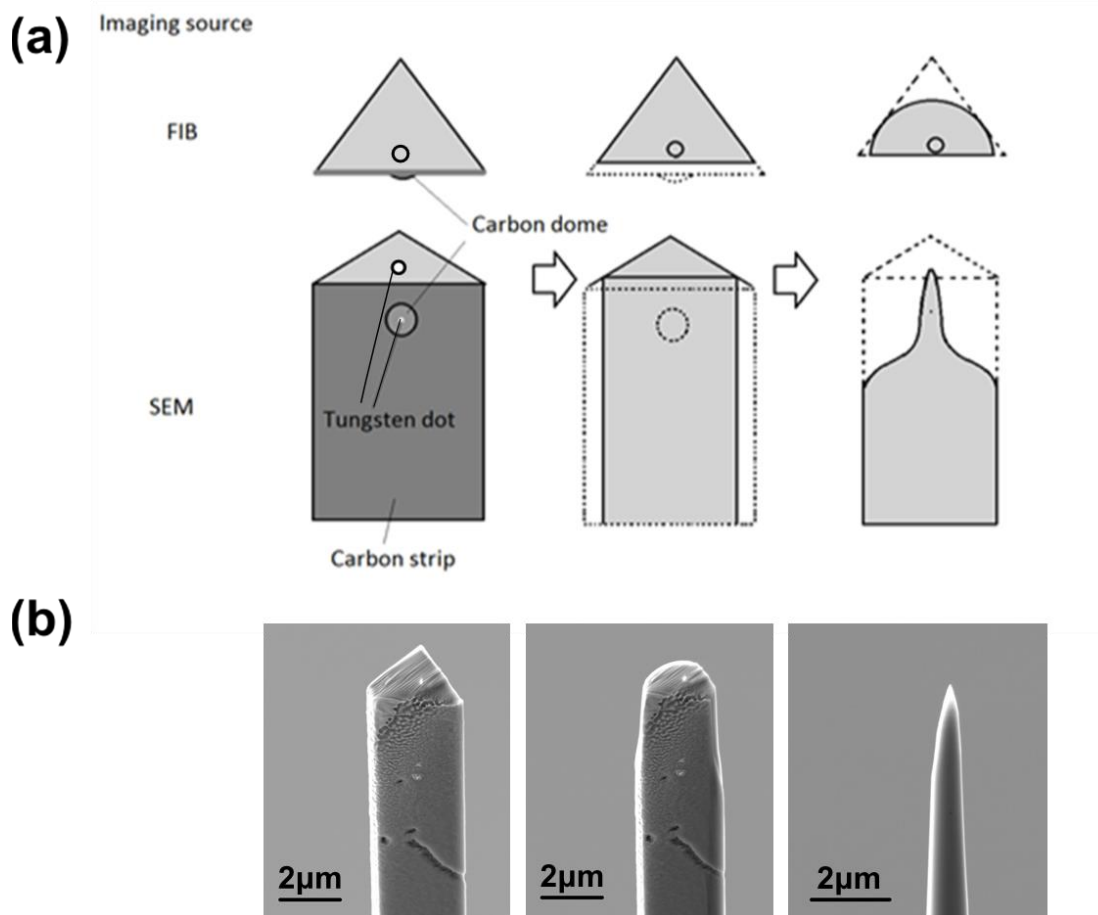
Figure 5 (a) A schematic illustration of the specimen sharpening process for an isolated dislocation: the first step is to remove the defect marking components and the majority of the dislocation pit by milling a rectangular pattern parallel to the marker surface. The wedge is then sharpened into an APT specimen by applying a series of annular milling patterns at various beam currents. (b) SEM images illustrating the specimen sharpening process for an isolated dislocation.

The specimen sharpening procedure for the grain boundary is broadly similar, as illustrated in Figure 6. First, a second fiducial tungsten dot is electron beam deposited at 0⁰ tilt on the triangular-shaped top surface of the wedge to mark the position of the end of the grain boundary. This gives two fiducial marks, one on the end of the wedge facing the FIB beam to aid with placement of the milling ring, and the second on the front face of the wedge facing the SEM column, so that the height of the defect can be monitored as the needle is sharpened, ensuring that the defect is within the APT analysis volume at the end of the sharpening procedure. The specimen is then tilted to 54⁰ and a similar rectangular cut is made at 80pA to the surface of the specimen to remove the tungsten line marking grain boundary, leaving behind only the tungsten dot. As before, the wedge is sharpened using an annular milling pattern at decreasing ion beam currents, with the pattern centre aligned with the tungsten dot. As noted previously, the direction of the grain boundary below the surface was not always perpendicular to the surface, and careful positioning of the annular milling pattern is necessary to ensure that the feature of interest remains in the volume in the final needle.
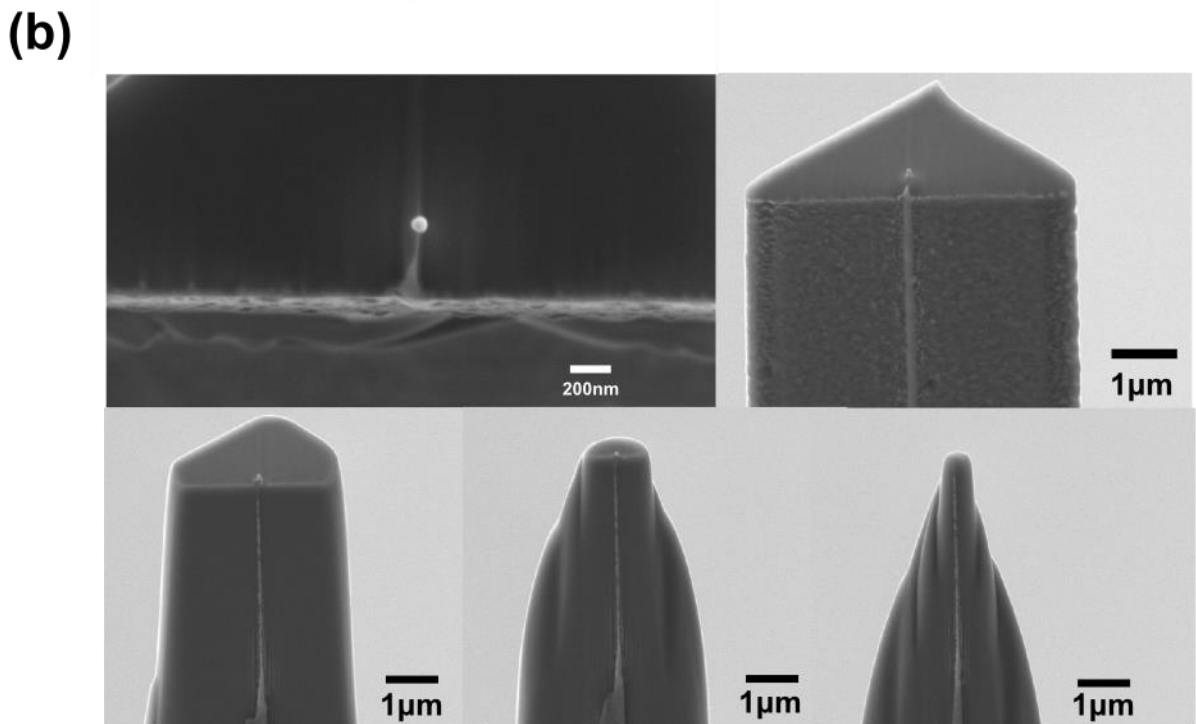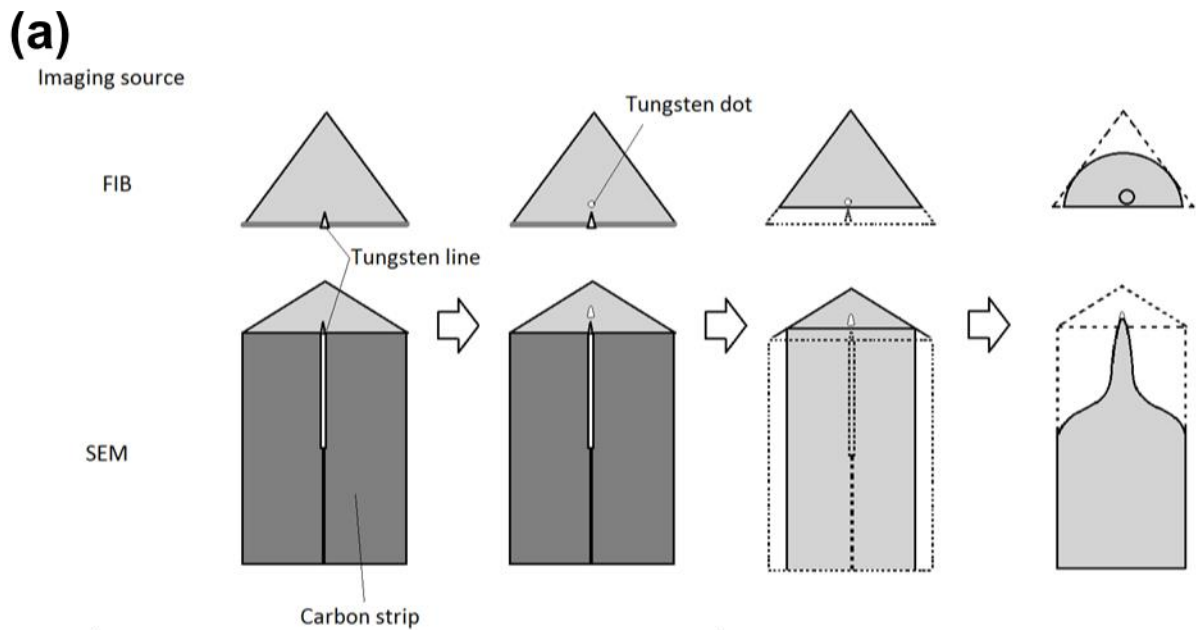
Figure 6. (a) A schematic illustration of the specimen sharpening process for a grain boundary. In the first step, a tungsten dot is deposited a small distance from the bottom of the grain boundary groove to mark the positon of the APT specimen's tip. The second step is to remove the defect-marking components by milling a rectangular pattern parallel to the marker surface. Finally, the APT specimen is fabricated by applying a series of annular milling patterns at various beam currents, with their centres aligned with the tungsten dot. (b) illustrates a series of SEM images showing the specimen sharpening process for a grain boundary.

Prior to APT analysis, the specimen is exposed to a low energy ion beam (5 kV 40 pA) to remove surface regions damaged by the ion beam during the previous steps[12]. The height of the specimen is usually reduced by about 100 nm by the low energy beam, but additional height can be removed if the extended defect is situated further down the specimen tip in order to ensure that it is within the analysed volume. This can be particularly advantageous when preparing specimens containing isolated dislocations.

4. Results and discussion

Using the methods described in this paper, two APT specimens were fabricated, incorporating a grain boundary and an isolated dislocation, respectively. The grain boundary specimen is extracted from a mc-Si sample that has been intentionally contaminated with gold. The isolated dislocation is taken from a mc-Si sample subjected to industrial standard phosphorus diffusion gettering (PDG). TEM images were taken prior to the low-energy ion beam cleaning stage.

4.1 Grain boundary characterisation

Figure 7 (a) shows a TEM composite of a specimen of gold-contaminated mc-Si containing a grain boundary running along the centre of the specimen; the grain to the right of the boundary appears to be darker than that to the left due to diffraction contrast, caused by the difference in their crystallographic orientation. Dark lines running at regular intervals along the grain boundary were observed when the specimen was rotated by 15° about the specimen axis, as shown in Figure 7 (b) and (c). These lines were found to disappear and reappear during the rotation and are only visible when the diffracting conditions in one or both grains are suitable to satisfy the g*b criterion, strongly indicating that these lines are dislocations [24].

Figure 7 (d) and (e) show the APT atom maps from the same sample, displaying for the distribution of Ni, N and C atoms (for visual clarity elemental Si atoms are not shown). The APT analysis is shown in two orientations, with the grain boundary plane normal and parallel to the imaging plane, respectively. These images indicate that the segregation of these elements to the grain boundary and associated dislocations are visible in the APT reconstruction, even though no Au was detected at this particular defect. Note that the dislocations visible in the APT images are not necessarily the first dislocations visible in the TEM image in Figure 7(c), and that due to the field of view of APT not all of the width of the needle visible in TEM is shown in the APT image. Two characteristic distributions of chemical species were observed at the grain boundary; (i) the enrichment of C and Ni at the grain boundary; and (ii) the segregation of Ni, C, N, and O at three particular regions along the grain boundary. All of these solute atoms with the exception of Ni were only detected in the APT analysis in the form of complex ions, namely SiN, SiC and SiO. Nickel was detected both as individual Ni atoms as well as NiC complex ions.
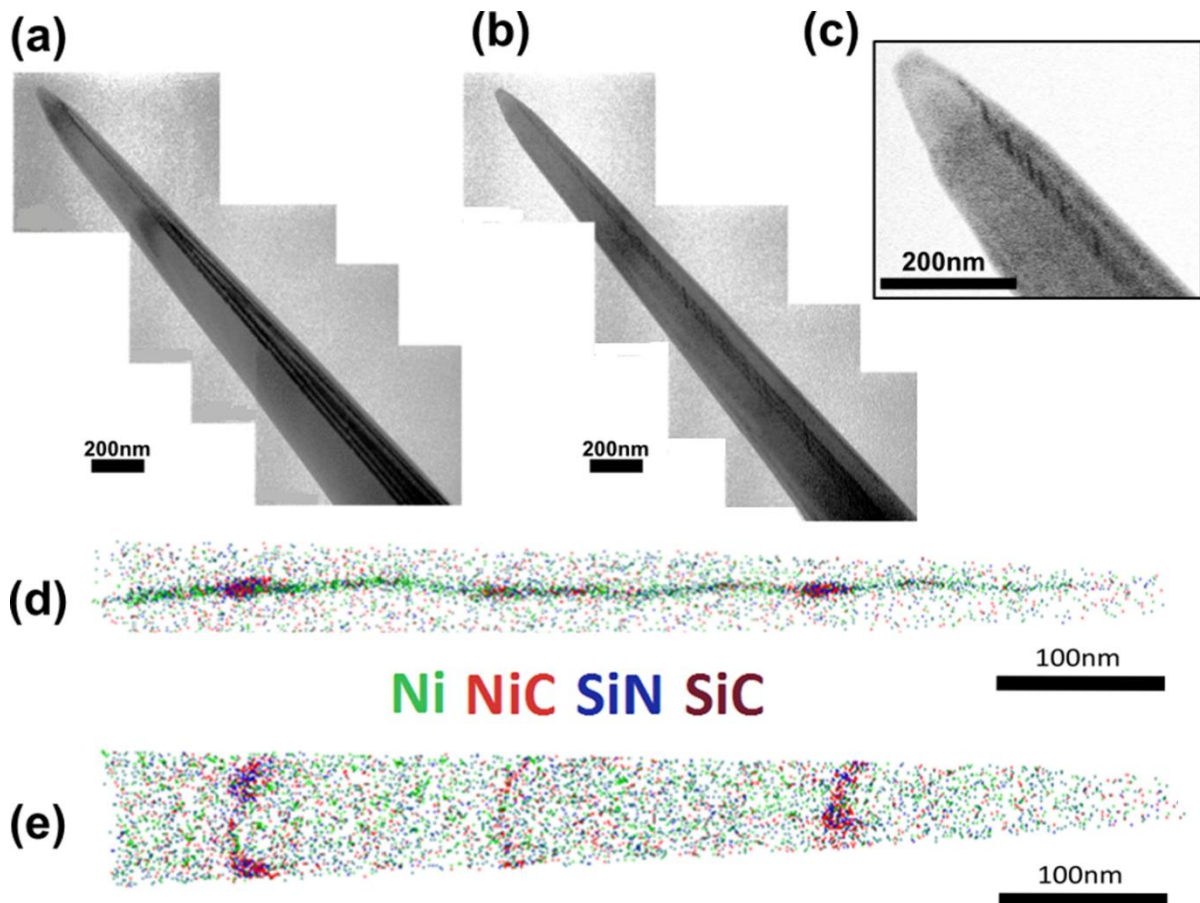
Figure 7. (a). BF images of the APT specimen containing a grain boundary at (a) 0° tilt and (b) 15° tilt. (c): a high magnification BF image of the top section of the specimen in (b). (d) and (e) show atom maps of the APT specimen containing a grain boundary taken from the gold-contaminated mc-Si sample. The reconstructions were taken at two different angles with the grain boundary plane in (d) and (e) being normal and parallel to the imaging plane, respectively. In addition, (d) shows a uniform distribution of Ni (light green) and SiC (dark green) throughout the grain boundary. The reconstruction in (e) shows segregation of NiC (red) and SiN (blue) to linear features at three distinct locations (marked by orange arrows) on the grain boundary plane.

4.2 Isolated dislocation characterisation

A similar correlative analysis was performed using TEM and APT for a specimen with an isolated dislocation taken from mc-Si material following a PDG process. Figure 8 (a), shows a bright field TEM image of the specimen. A dark dot is observed, with a bright region on one side of the dot and a dark region on the other side, which is similar to TEM images of edge dislocations[25,26]. In the subsequent APT reconstruction of the same specimen presented in Figure 8 (b) and (c), two spherical Ni clusters with a diameter ~10 nm are observed decorating the defect. The distance between these clusters from centre-to-centre is approximately 35 nm. As with the grain boundary sample in Figure 7, the higher magnification APT image shows a narrower tip than the TEM image due to the field of view of the LEAP instrument – as the tip gets wider, some of the outer regions of the shank are not visible in the APT data. The presence of Ni clusters after PDG is significant, suggesting that nickel atoms present at dislocations are resistant to gettering. Further study is required to characterise the significance of nickel clusters on the electrical properties of the material.
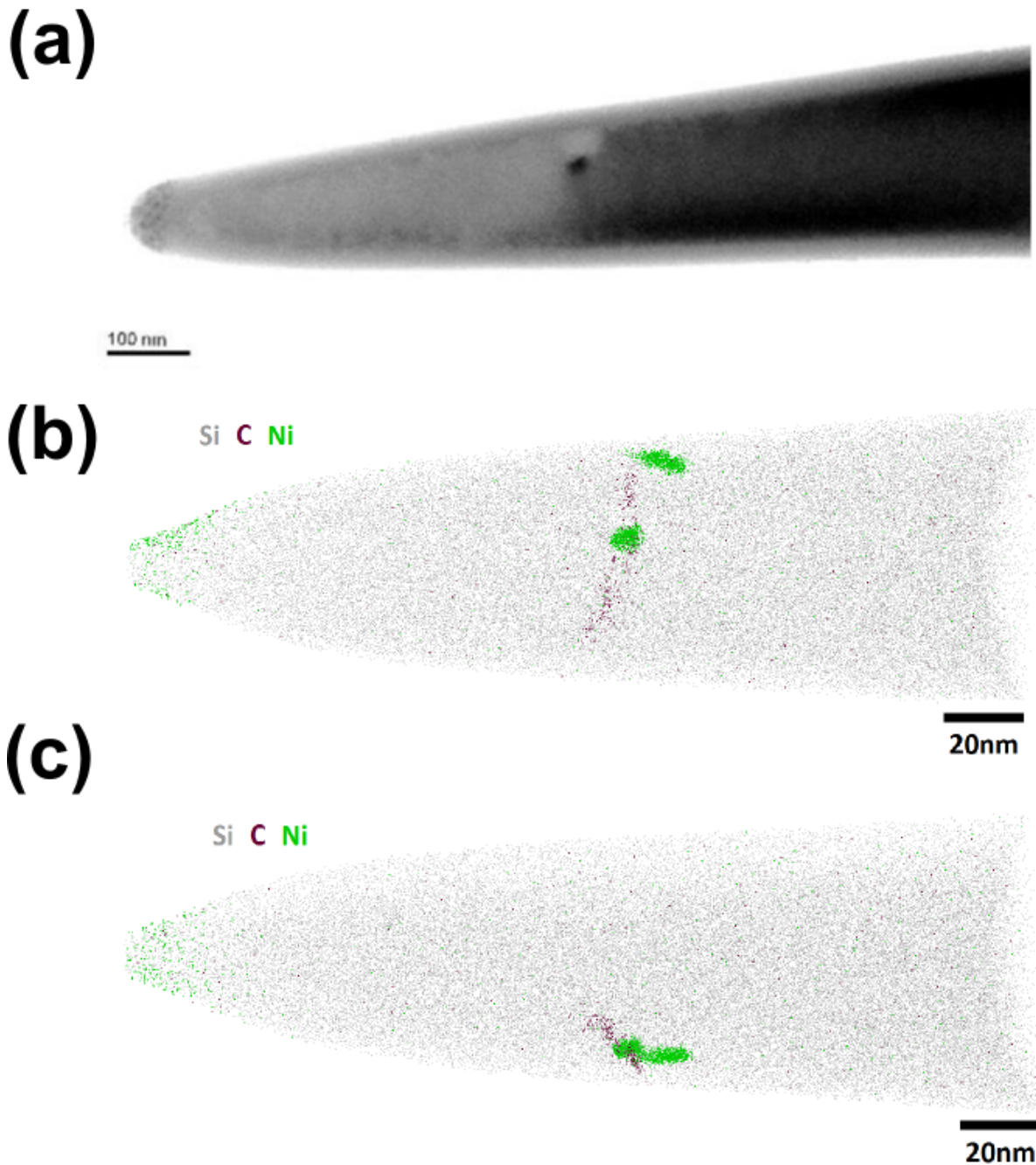
11

Figure 8. (a) BF TEM image of an APT specimen containing an isolated dislocation taken from the post-PDG mc-Si wafer. (b) and (c) Atom maps at different rotations of the post-PDG specimen showing two Ni clusters (green) decorating the along the dislocation line marked by dark purple carbon atoms. A limited number of Si atoms are shown to aid visual interpretation.

The ability to observe and characterise such nanoscale impurities from lone dislocations proves the effectiveness of this advanced specimen preparation method. It would be significantly more difficult to intentionally characterise such a small isolated feature using the standard lift out method. Due to the large distances between each dislocation away from the GB in mc-Si, the chances of a random 100x200 nm APT specimen containing such a feature without the etching, marking and precise annular milling steps shown here are extremely low. In addition, whilst segregation of impurities to mc-Si grain boundaries has previously been demonstrated using APT[19], the orientation of the GB

perpendicular to the analysis direction using this method means that an increased length of the GB can be incorporated within a single APT analysis.

5. Conclusions

Atom Probe Tomography (APT) is an increasingly critical tool for characterising the chemistry of many materials at the atomic scale. In the case of small isolated defects, such as isolated dislocations in multicrystalline silicon, preparing a needle-shaped APT specimen with a tip radius of 50-100 nm whilst still retaining the region of interest at the tip apex is challenging. Novel specimen preparation methods for atom probe analysis of specifically selected defects were developed using a FIB-SEM dual beam system. The mc-Si material was etched using a Secco etch for a short period of time to expose etch pits where isolated dislocations and grain boundaries are present on the surface.

The effectiveness of this site-specific FIB preparation method has been demonstrated for a grain boundary specimen in a mc-Si material contaminated with gold, and an isolated dislocation subjected to PDG contamination. Bright field TEM images were used prior to APT analysis to confirm the presence of defects in both specimens. Subsequent APT results showed it was possible to observe even very small decorations of impurities at these defects. Whilst this has been previously demonstrated for grain boundaries, the observation of two 10 nm Ni precipitates at the site of an isolated dislocation is unique to this preparation method and proves its effectiveness in successfully producing APT specimens containing individual defects on the nm scale within the apex of the specimen.

This preparation method provides much more control over the region of interest studied, greatly increasing the amount of information that can be inferred about the nature of impurity diffusion to defects, and should be of significant benefit to materials characterisation of mc-Si. It is also applicable to many other materials, where the defect can be marked using a suitable etchant or other method, and therefore the grain boundary or individual dislocation can be lifted out using this method for atomic-scale characterisation using APT.

Acknowledgements

References

[1] Green,M.A., Emery, K. Hishikawa, Y., Warta, W. & Dunlop, E.D. (2016) *Solar cell efficiency tables (Version 47)*, Progress in Photovoltaics 24 (1) pp.3-11

[2] Istratov, A.A., Buonassisi, T., McDonald, R.J., Smith, A.R., Schindler, R, Rand, J.A., Kalejs, J.P & Weber, E.R. (2003) *Metal content of multicrystalline silicon for solar cells and its impact on minority carrier diffusion length*, J. Appl. Phys. 94, 6552

[3] Fujiwara, K., Pan, W., Usami, N., Sawada, K., Tokairin, M., Nose, Y., Nomura, A, Shishido, T. & Nakajima, K. (2006). *Growth of structure-controlled polycrystalline silicon ingots for solar cells by casting*, Acta Materialia, 54 pp.3191-3197

[4] Lan, C.W., Lan, W.C., Lee, T.F., Yu, A., Yang, Y.M., Hsu, W.C., Hsu, B. & Yang, A. (2012) *Grain control in directional solidification of photovoltaic silicon*, Journal of Crystal Growth, 360, pp.68-75

[5] Yang, Y.M., Yu, A., Hsu, B., Hsu, W.C., Yang, A & Lan, C.W. (2013) *Development of high-performance multicrystalline silicon for photovoltaic industry*, Progress in Photovoltaics 23 (3), pp.340-351

[6] Coletti, G., Bronsveld, P.C.P., Hahn, G., Warta, W. Macdonald, D., Ceccaroli, B., Wambach, K., Quang, N.L. & Fernandez, J.M. (2011), *Impact of metal contamination in silicon solar* cells, Advanced Functional Materials 21 (5), pp.879-890

[7] Davis, J.R., Rohatgi, A., Hopkins, R.H., Blais, P.D., Rai-Choudhury, P., McCormick, J.R.& Mollenkopf, H.C. (1980), *Impurities in silicon solar cells,* IEEE Transactions on Electron Devices 27 (4), pp.677-687

[8] Buonassisi, T., Istatov, A.A., Pickett, M.D., Heuer, M., Kalejs, J.P., Hahn, G., Marcus, M.A., Lai, B., Cai, Z., Heald, S.M., Ciszek, T.F., Clark, R.F., Cunningham, D.W., Gabor, A.M., Jonczyk, R., Narayanan, S., Sauar, E. & Weber, E.R. (2006) *Chemical natures and distributions of metal impurities in multicrystalline silicon materials,* Progress in Photovoltaics, 14 (6), pp.513-531

[9] Bertoni, M.I., Fenning, D.P., Rinio, M. Rose, V., Holt, M., Maser, J. & Buonassisi, T. (2011) *Nanoprobe X-ray fluorescence characterisation of defects in large-area solar cells*, Energy Environ.Sci, 4, pp.4252-4257

[10] Larson, D.J., Prosa, T.J., Perea, D.E., Inoue, K. & Mangelinck, D. (2016). *Atom probe tomography of nanoscale electronic materials*, MRS Bulletin 41, pp.30-34

[11] Kellogg, G.L. & Tsong, T.T. (1980). *Pulsed-laser atom-probe field-ion microscopy*. Journal of Applied Physics, 51 (2), pp. 1184-1193.

[12] Thompson, K., Lawrence, D., Larson, D. J., Olson, J. D., Kelly, T. F., & Gorman, B. (2007). *In situ site-specific specimen preparation for atom probe tomography*. Ultramicroscopy, 107 (2), pp.131-139.

[13] Saxey, D. W., Cairney, J. M., McGrouther, D., Honma, T., & Ringer, S. P. (2007). *Atom probe specimen fabrication methods using a dual FIB/SEM*. Ultramicroscopy, 107 (9), pp.756-760.

[14] Larson, D.J., Foord, D.T., Petford-Long, A.K., Liew, H., Blamire, M.G., Cerezo, A. and Smith, G.D.W. (1999). *Field-ion specimen preparation using focused ion-beam milling*. Ultramicroscopy, 79 (1-4), pp.287-293

[15] Thompson, K., Bunton, J.H., Kelly, T.F., & Larson, D.J. (2006). *Characterization of ultralow-energy implants and towards the analysis of three-dimensional dopant distributions using three-dimensional atom-probe tomography*, Journal of Vacuum Science and Technology B, Nanotechnology and Microelectronics: Materials, Processing, Measurement and Phenomena. 24, pp.421-427

[16] Thompson, K., Booske, J.H., Larson, D.J. & Kelly, T.F. (2005). *Three-dimensional atom mapping of dopants in Si nanostructures.* Applied Physics Letters. 87 (5), 052108

[17] Hoummada, K., Mangelinck, D., Gault, B. & Cabié, M. (2011). *Nickel segregation on dislocation loops in implanted silicon.* Scripta Materialia. 64 (5), pp. 378-381

[18] Duguay, S., Colin, A., Mathiot, D., Morin, P. and Blavette, D. (2010). *Atomic-scale redistribution of dopants in polycrystalline silicon layers*. Journal of Applied Physics. 108 (3), 034911

[19] Stoffers, A., Cojocaru-Mirédin, O., Seifert, W., Zaefferer, S., Riepe, S., & Raabe, D. (2015). *Grain boundary segregation in multicrystalline silicon: correlative characterization by EBSD, EBIC, and atom probe tomography.* Progress in Photovoltaics: Research and Applications. 23 (12), pp.1742-1753

[20] Felfer, P. J., Alam, T., Ringer, S. P., & Cairney, J. M. (2012). *A reproducible method for damage-free site-specific preparation of atom probe tips from interfaces*. Microscopy research and technique, 75 (4), pp.484-491.

[21] Kang, J.S. & Schroder, D.K. (1989). *Gettering in silicon*. Journal of Applied Physics, 65 (8), pp. 2974-2985.

[22] Stolwijk, N.A., Schuster, B., Hölzl, J., Mehrer, H. & Frank, W. (1983). *Diffusion and solubility of gold in silicon*. Physica B+C, 116(1-3), pp.335-342

[23] Kern, W. & Puotinen, D. (1970). *The RCA Clean (revision 3),* RCA Rev., 31 (2) pp.187

[24] Crimp, M. A., Simkin, B. A., & Ng, B. C. (2001). *Demonstration of the g· bxu= 0 edge dislocation invisibility criterion for electron channelling contrast imaging*. Philosophical magazine letters, 81 (12), pp.833-837.

[25] Menter, J. (1956). *The direct study by electron microscopy of crystal lattices and their imperfections*. In Proceedings of the Royal Society of London A: Mathematical, Physical and Engineering Sciences (Vol. 236, No. 1204, pp.119-135). The Royal Society.

[26] Yang, H., Lozano, J. G., Pennycook, T. J., Jones, L., Hirsch, P. B., & Nellist, P. D. (2015). *Imaging screw dislocations at atomic resolution by aberration-corrected electron optical sectioning*. Nature Communications, 6.